

Mixed Multilayered Vertical Heterostructures Utilizing Strained Monolayer WS₂

*Yuewen Sheng¹, Wenshuo Xu¹, Xiaochen Wang¹, Zhengyu He¹, Youmin Rong¹, Jamie H.
Warner^{1*}*

¹Department of Materials, University of Oxford, Parks Road, Oxford, OX1 3PH, United
Kingdom

**Jamie.warner@materials.ox.ac.uk;*

Abstract

Creating alternating layers of 2D materials forms vertical heterostructures with diverse electronic and opto-electronic properties. Monolayer WS₂ grown by chemical vapour deposition can have inherent strain due to interactions with the substrate. The strain modifies the band structure and properties of monolayer WS₂ and can be exploited in a wide range of applications. We demonstrate a non-aqueous transfer method for creating vertical stacks of mixed 2D layers containing a strained monolayer of WS₂, with Boron Nitride and Graphene. The 2D materials are all grown by CVD, enabling large area vertical heterostructures to be formed. WS₂ monolayers grown by CVD directly on Si substrates with SiO₂ surface are easily washed off by water and this makes aqueous based transfer methods challenging for creating vertical stacks on the growth substrate. 2D hexagonal Boron Nitride films are used to provide an insulating layer that limits interactions with a top graphene layer and preserve the strong photoluminescence from the WS₂. This transfer method is suitable for layer by layer control of 2D material vertical stacks and is shown to be possible for all CVD grown samples, which

opens up pathways for the rapid large scale fabrication of vertical heterostructure systems with atomic thickness depth control and large area coverage.

KEYWORDS: Graphene, WS₂, Boron Nitride, vertical heterostructures, 2D materials.

Introduction

Two-dimensional (2D) transition metal dichalcogenides (TMDs), such as Tungsten disulfide (WS₂) and Molybdenum disulfide (MoS₂), have recently drawn attention due to their unique electrical and optical properties.^{1–10} The van der Waals heterostructures based on TMDs and other 2D materials, such as graphene and hexagonal boron nitride (h-BN), are believed to be the fundamental platform for many important future device applications including transistors, solar cells, light-emitting diodes and lasers.^{11–26} These 2D heterostructures can be realized by either transfer^{13–23} or direct growth.^{24–27} As for the transfer approach, the dry transfer method, such as the Polydimethylsiloxane (PDMS) stamping technique, is often used by research groups.^{16–21} By using the dry transfer method, one 2D material can be transferred onto another 2D material, which was either grown or exfoliated on a Silicon chip with a layer of Silicon dioxide on top (SiO₂/Si), for device fabrication.

The development of transfer methods is essential for the layer by layer van der Waals reassembly.¹¹ Schneider et al.²⁸ reported a transfer method in 2010, which occurs through the intercalation of a layer of water between a hydrophilic substrate and a hydrophobic nanostructure (for example, graphene and carbon nanotubes) locked within a hydrophobic polymer thin film. This led to a so-called surface energy assisted perfect transfer.²⁹ They successfully detached the Polystyrene (PS) /MoS₂ film (hydrophobic) from a sapphire substrate (hydrophilic) by water penetration. A similar transfer technique was demonstrated by Xu et

al.³⁰, they delaminated WS₂ from sapphire substrates via capillary force in water. Recent studies³¹ also reported using polydimethylsiloxane (PDMS) (as the carrier polymer) and cold water to lift off the synthesized MoS₂ films from the SiO₂/Si substrate. However, this requires the presence of a water-soluble layer beneath the as-grown films, which is not typical in the synthetic approaches for TMDs.

Recent reports show that water can easily detach TMDs from a hydrophilic substrate, such as SiO₂, making it difficult to transfer other 2D materials on top of as-grown TMDs by the standard wet transfer method that was widely used for graphene.^{32–34} A dry transfer method (PDMS)^{16–21} can be used to form a heterostructure based on TMDs. Some success has been achieved for monolayer TMD films on sapphire using a wet transfer method to build the 2D heterostructures, but this approach does not work consistently with SiO₂ surfaces.²² It might be the case that the synthesized monolayer film adhered better to the growth substrate, which then hinders the water penetration and allows it remain undamaged on the surface.²⁹

One important aspect for atomically thin TMDs is their flexibility, which is better suited for strain engineering compared with other bulk semiconductors.^{35,36} It was reported that the local strain in as-grown TMD samples normally arises from the CVD growth procedures that end with a fast-cooling process due to the difference in the coefficient of thermal expansion between the substrate and as-prepared material, and the tensile strain can be released by a transfer process to another substrate.³⁷ Tuning the band structure and carrier transport properties by applying a strain through bending of materials on flexible substrates or through lattice mismatch between substrates and samples has been explored recently, and it can be used to significantly improve their optical and electronic properties.^{16,35–40} It has been predicted that tunable photonic devices and solar cells with better energy band matching can be realized by

building multilayer 2D heterostructures based on strained TMDs.^{38,41} Building layer-by-layer vertical heterostructures containing a strained TMD layer has been challenging due to the standard aqueous based transfer processes washing off the TMDs from the growth substrate. It is important to develop a non-aqueous transfer approach that allows other 2D crystals to be assembled on top of the strained TMDs to build multi-layered vertical heterostructures.

Here we introduced a novel alcohol-based approach to the transfer of 2D materials, such as h-BN and graphene, on top of WS₂ directly grown on a Si substrate with SiO₂ surface. Using isopropanol (IPA) instead of water enables layer-by-layer transfer of 2D material onto CVD grown strained TMDs on hydrophilic substrates, such as sapphire and SiO₂/Si without using PDMS. The non-aqueous transfer method is also suitable for transferring monolayer WS₂ from its growth substrate to other substrates, releasing the strain and building vertical 2D heterostructures with different stacking order. Optical microscopy, scanning electron microscopy (SEM), Raman spectroscopy and Photoluminescence (PL) spectroscopy was used to characterize the h-BN/WS₂, graphene/h-BN/WS₂ and WS₂/graphene stacks prepared by both the standard aqueous-based wet transfer method and our non-aqueous sliding transfer approach.

Results and discussion

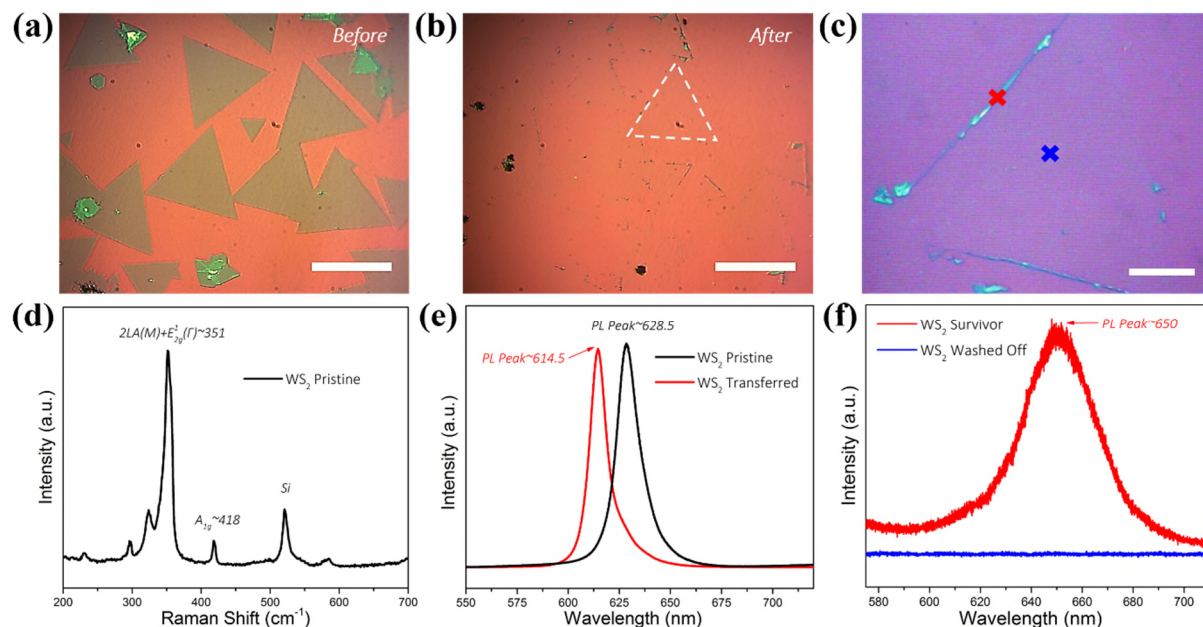


Figure 1. Monolayer WS₂ crystals easily removed from the substrate by immersion in DI water.

Optical images of WS₂ before (a) and after (b) submerged in DI water. The white dashed area shows where a WS₂ triangle used to be. The Scale bar: 100μm. (c) Zoomed-in optical image of WS₂ residues on SiO₂/Si after being in contact with DI water. Scale bar: 30μm. (d) Raman spectrum of as-grown monolayer WS₂ on SiO₂/Si. (e) PL spectra of as-grown monolayer WS₂ (black line) and transferred WS₂ (red line) on SiO₂/Si, respectively. (f) PL spectra of the marked spots with corresponding colored crosses in (c), showing that the material left on the surface is not monolayer, but multilayer WS₂.

All 2D materials used in this study were grown by CVD. Figure 1(a) presents the optical image of our as-grown monolayer WS₂ crystals on SiO₂/Si. Figure 1(d) shows the Raman spectra of the as-grown monolayer WS₂ domain on SiO₂/Si. A peak at 351 cm⁻¹ was observed and assigned to the 2LA+E_{2g}¹ mode for monolayer WS₂, while the peak at 418 cm⁻¹ corresponds to the A_{1g} mode, consistent with our previous reports.^{42–44} Figure 1(e) compares the PL spectra of as-grown (~628.5nm) and transferred (~614.5nm) monolayer WS₂ on SiO₂/Si. A blue shift

of 14nm was observed after transfer, which is thought to be mostly caused by the released strain. The 2D vertical heterostructure was first prepared by transferring a layer of 2D material using a standard wet transfer approach³² onto another layer that was grown directly on SiO₂/Si. During the transfer process, it was found that most of the WS₂ crystals were washed away after being immersed in deionized (DI) water, leaving traces of some WS₂ triangles and hexagons on the surface. Figures 1(a) and (b) show the optical images of WS₂ domains before and after being submerged in DI water. The white dashed triangle indicates where a WS₂ domain used to be. Figure 1(c) shows the zoomed-in optical image of the outline of some WS₂ crystals left after transfer. From the PL spectra as shown in Figure 1(f), it can be confirmed that most of the monolayer WS₂ was detached from the substrate. The low PL intensity and peak position (~650nm) of the WS₂ residue near the edge indicates that the material left on the surface is not monolayer, but multilayer WS₂ (Supporting Information Figure S1), possibly formed by back folding of some monolayer regions. According to the optical image (Figure 1(b)), it seems that there is still some residue of material at the point where the WS₂ triangles or hexagons used to be before exposure to DI water. Raman spectroscopy was then used to determine that no W-oxides was left on the surface and that most of the monolayer WS₂ was completely washed off after exposure to water (Supporting Information Figure S2).

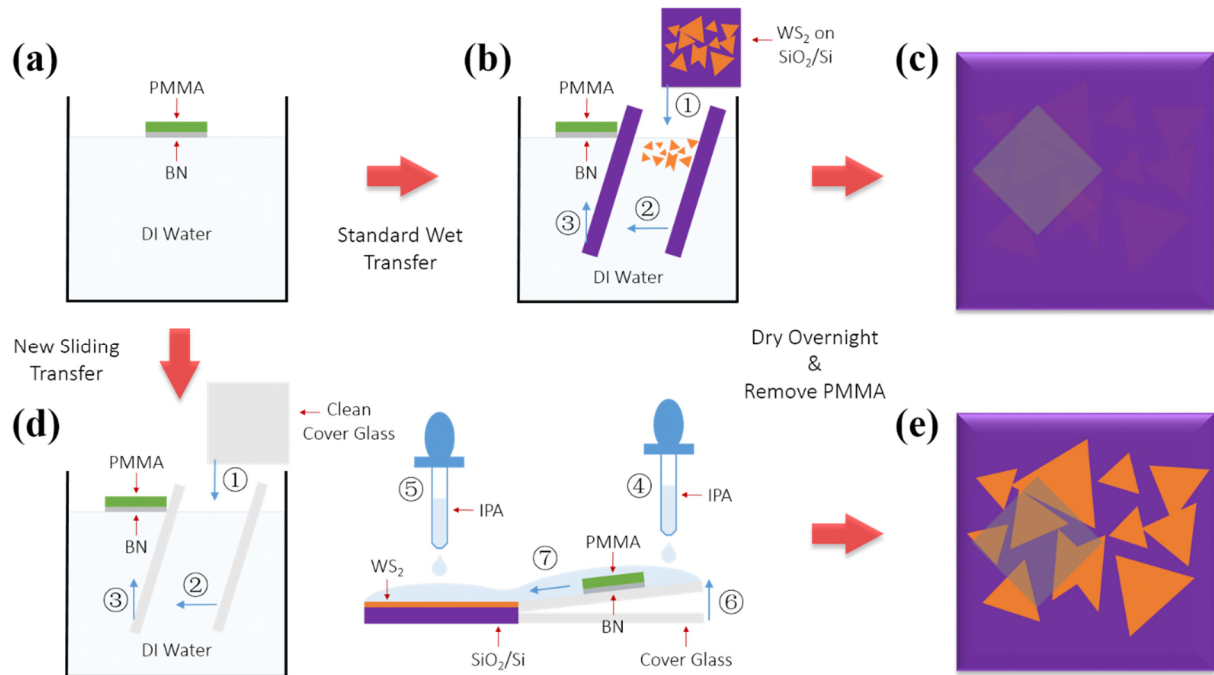


Figure 2. Schematic illustration of the non-aqueous sliding transfer method and the standard aqueous wet transfer process. (a) After all the cleaning processes, the PMMA/h-BN stack was floating on DI water. (b) The standard wet transfer involves (1) suspending the WS₂/SiO₂/Si chip in the DI water, (2) pushing it towards the stack and (3) scooping the stack onto the WS₂/SiO₂/Si chip. (c) It was found that most of the WS₂ crystals were washed off when soaked in DI water. (d) The sliding transfer process includes (1) dipping a piece of clean cover glass into DI water, (2) pushing it towards the stack, (3) scooping the stack onto the cover glass, (4) wetting the cover glass with some IPA, (5) dropping IPA onto the WS₂/SiO₂/Si chip and keep it horizontal on the desk, (6) resting one side of the cover glass on the edge of the chip and lifting the other side up slightly and (7) allowing the stack to slide down very slowly. (e) All the WS₂ crystals remain intact after removing PMMA.

Figure 2 shows the schematic illustration of standard aqueous wet transfer process and non-aqueous sliding transfer method. Taking h-BN/WS₂ as an example, after etching the Cu away and removing the etchant via several cleaning steps, the PMMA/h-BN stack was transferred to DI water, as shown in Figure 2(a). As can be seen from Figure 2(b), the standard

wet transfer method involves DI water when scooping the PMMA/h-BN stack onto WS₂/SiO₂/Si substrate, and most of the WS₂ crystals were found to be washed off after this process (Figure 2(c)). Therefore, a new transfer process has been introduced here in order to solve this problem. Figure 2(d) shows the schematic illustration of the non-aqueous sliding transfer approach that eliminates the need to bring WS₂ monolayers in contact with water. First, a thin cover-glass slide was used to collect the PMMA/h-BN stack after all the cleaning process. Then some IPA is added to surface of the cover glass, allowing the solution to draw away the DI water between the cover glass and the stack. In the meantime, some IPA is dropped onto the WS₂/SiO₂/Si, which is kept horizontal on the desk. With one side of the cover glass resting on the edge of the Si chip, the other end of the cover glass is lifted up so that the PMMA/h-BN stack slides across to the Si chip slowly. Then the whole stack is left to dry in a fume hood overnight and is then baked at 175°C for 15 minutes. All the WS₂ crystals remain intact after the PMMA removal by acetone (Figure 2(e)).

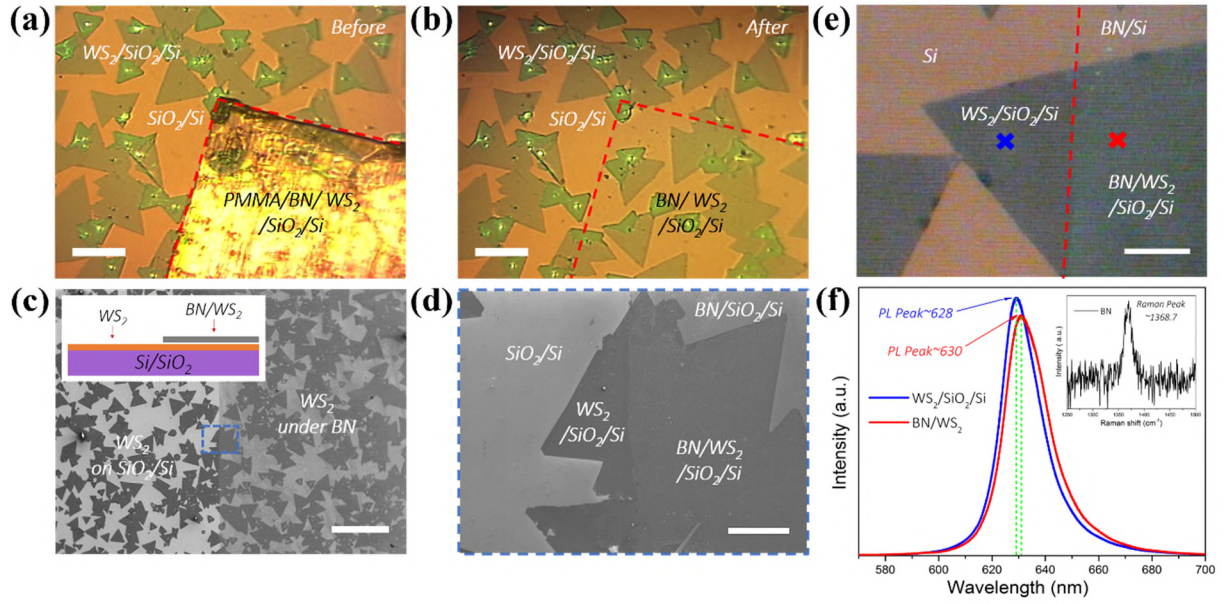


Figure 3. Characterization of an h-BN/WS₂ stack prepared via the sliding transfer approach.

Optical images of WS₂ underneath h-BN before (a) and after (b) PMMA removal. The red dashed line indicates the boundary of h-BN. Scale bar: 60 μ m. (c) SEM image of WS₂ crystals on SiO₂/Si with and without h-BN on top. Scale bar: 0.5mm. Inset shows the schematics of the h-BN/WS₂ stack. (d) SEM image of zoomed-in blue dashed region in (c), showing WS₂ domains partially under h-BN. Scale bar: 50 μ m. (e) Zoomed-in optical image of WS₂ crystals on SiO₂/Si after transferring a layer of h-BN using the new transfer method. Scale bar: 20 μ m. (f) PL spectra of the marked spots with corresponding colored crosses in (e), showing the difference in PL signal between WS₂ with and without h-BN on top. The inset is the Raman spectra of multilayer h-BN.

Figure 3(a) shows the optical image of WS₂ samples before removing PMMA using acetone, with the PMMA/h-BN stack indicated by a red dashed line. As can be seen from Figure 3(b), all the WS₂ crystals remain intact after PMMA removal. Due to h-BN's high transparency, there is almost no difference in contrast between the area with BN and without BN under the optical microscope. The inset in Figure 3(c) shows a schematic of the h-BN/WS₂ stack. According to the SEM image shown in Figure 3(c), it can be confirmed that a layer of h-BN

was transferred onto the WS₂ using the sliding transfer approach. Figure 3(d) presents the SEM image of zoomed-in blue dashed area in Figure 3(c). Figure 3(e) shows the zoomed-in optical image of WS₂ crystals with and without h-BN on top. As can be seen from Figure 3(f), the WS₂ underneath the h-BN has weaker PL intensity with broader full width at half maximum (FWHM) than the one on SiO₂/Si. The PL peak position has barely changed with only a slight redshift from 628nm to 630nm after all the transfer process. The existence of an h-BN layer transferred on WS₂ was further confirmed by Raman spectroscopy. The inset in Figure 3(f) shows the characteristic Raman vibration mode of the h-BN film lying above the WS₂ domains, which was measured to be around 1368.7 cm⁻¹, indicating multilayer h-BN (Supporting Information Figure S3).

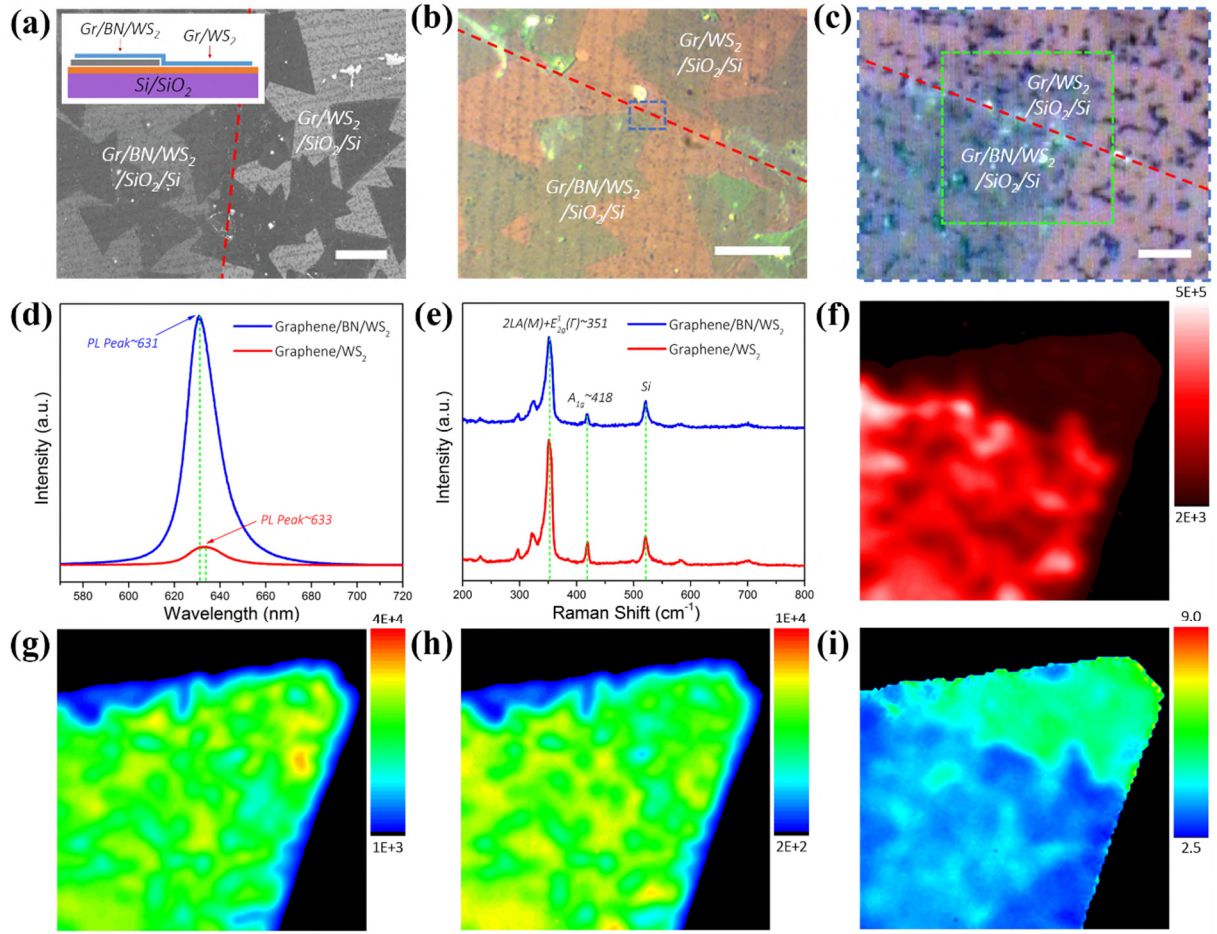


Figure 4. Characterization of a graphene/h-BN/WS₂ stack prepared by the non-aqueous sliding transfer approach. (a) SEM image of WS₂ crystals on SiO₂/Si after transferring a layer of graphene on top of the h-BN/WS₂ stack. The left side is covered with a layer of h-BN while the right side is not. Scale bar: 100μm. The Inset shows a schematic of the graphene/h-BN/WS₂ stack. (b) Optical image of graphene/h-BN/WS₂ stack. The red dashed line indicates the boundary of h-BN. Scale bar: 100μm. (c) Optical image of zoomed-in blue dashed area in (b). The green dashed square indicates the region for PL and Raman mapping. Scale bar: 10μm. (d) PL spectra of graphene/WS₂ stack with and without h-BN in between, showing a large PL quenching when there is no h-BN in between. (e) Raman spectra obtained from graphene/h-BN/WS₂ stack compared with the graphene/WS₂ stack, with highlighted Si peak and WS₂ characteristic peaks, 2LA+E_{2g}¹ and A_{1g}. (f) PL mapping obtained from the green dashed region in (c). The integrated photo emission intensity from wavelengths of 600 to 660nm is shown. (g-

i) Raman mapping obtained from the same graphene/h-BN/WS₂ region, highlighted with the green dashed line in (c), showing the integrated 2LA+E_{2g}¹ peak intensity from 330 to 370cm⁻¹, the integrated A_{1g} peak intensity from 400 to 430cm⁻¹ and the ratio of integrated 2LA+E_{2g}¹ peak intensity (330 to 370cm⁻¹)/integrated A_{1g} peak intensity (400 to 430cm⁻¹), respectively.

To further illustrate the flexibility of our non-aqueous transfer method in preparing mixed vertical stacked 2D heterostructures with a variety of 2D materials, a layer of graphene was then transferred onto the as-prepared h-BN/WS₂ stack using the non-aqueous transfer method. The graphene film is mostly bilayer with 15% area of multilayer graphene strips (Supporting Information Figure S4). The inset in Figure 4(a) presents a schematic diagram of the graphene/h-BN/WS₂ stack. The SEM image in Figure 4(a) shows WS₂ crystals with a layer of graphene on top. The left area indicated by the red dashed line was covered by a layer of h-BN, showing different contrast compared to the right region. Figure 4(b) shows the optical image of graphene/h-BN/WS₂ stack and Figure 4(c) is the zoomed-in optical image of the blue dashed area in Figure 4(b), showing almost no difference in contrast due to h-BN's high transparency under visible light. The red dashed line indicates the boundary of h-BN. Again, Raman and PL spectroscopy were used to characterize the graphene/h-BN/WS₂ stack prepared by the non-aqueous transfer method. As can be seen from Figure 4(d), under the same excitation laser power and acquisition time, it was found that the integrated PL intensity is about 12 times stronger from the graphene/WS₂ stack with h-BN in between than that without the h-BN separator. The drastic PL quenching observed results from the charge transfer between WS₂ and graphene, which is in agreement with the literature.⁴⁵ Figure 4(e) shows the Raman spectra obtained from graphene/WS₂ and graphene/h-BN/WS₂, both showing the peaks centered at 351 and 418cm⁻¹, which correspond to the WS₂ 2LA+E_{2g}¹ and A_{1g} Raman modes,

respectively. Furthermore, Figures 4(f-i) present PL and Raman intensity maps of the same region, the green dashed square in Figure 4(c). The whole area mapped was covered by a layer of graphene on top, but only part of it has a layer of h-BN in between, which is indicated by a red dashed line. Raman mapping of the $2\text{LA}+\text{E}_{2\text{g}}^1$ peak (Figure 4(g)) shows a relatively uniform integrated intensity over the area, while the integrated intensity of graphene/h-BN/ WS_2 area at the $\text{A}_{1\text{g}}$ Raman vibrating mode (Figure 4(h)) is slightly higher than that of the graphene/ WS_2 region, which leads to a different ratio of integrated $2\text{LA}+\text{E}_{2\text{g}}^1$ peak intensity ($330\text{-}370\text{cm}^{-1}$)/integrated $\text{A}_{1\text{g}}$ peak intensity ($400\text{-}430\text{cm}^{-1}$), as shown in Figure 4(i). The ratio is around 3 for the area with h-BN and about 5 for the region without. In addition, significant variations were seen in the PL mapping (Figure 4(f)) and it can be confirmed that the PL integrated intensity of the region without a layer of h-BN in between is much lower than the area with h-BN. The boundary of h-BN can be clearly distinguished, which means that by applying this transfer method, both h-BN and graphene can be assembled onto as-grown CVD WS_2 and h-BN can be an effective insulating layer which prevents interactions between WS_2 and graphene.

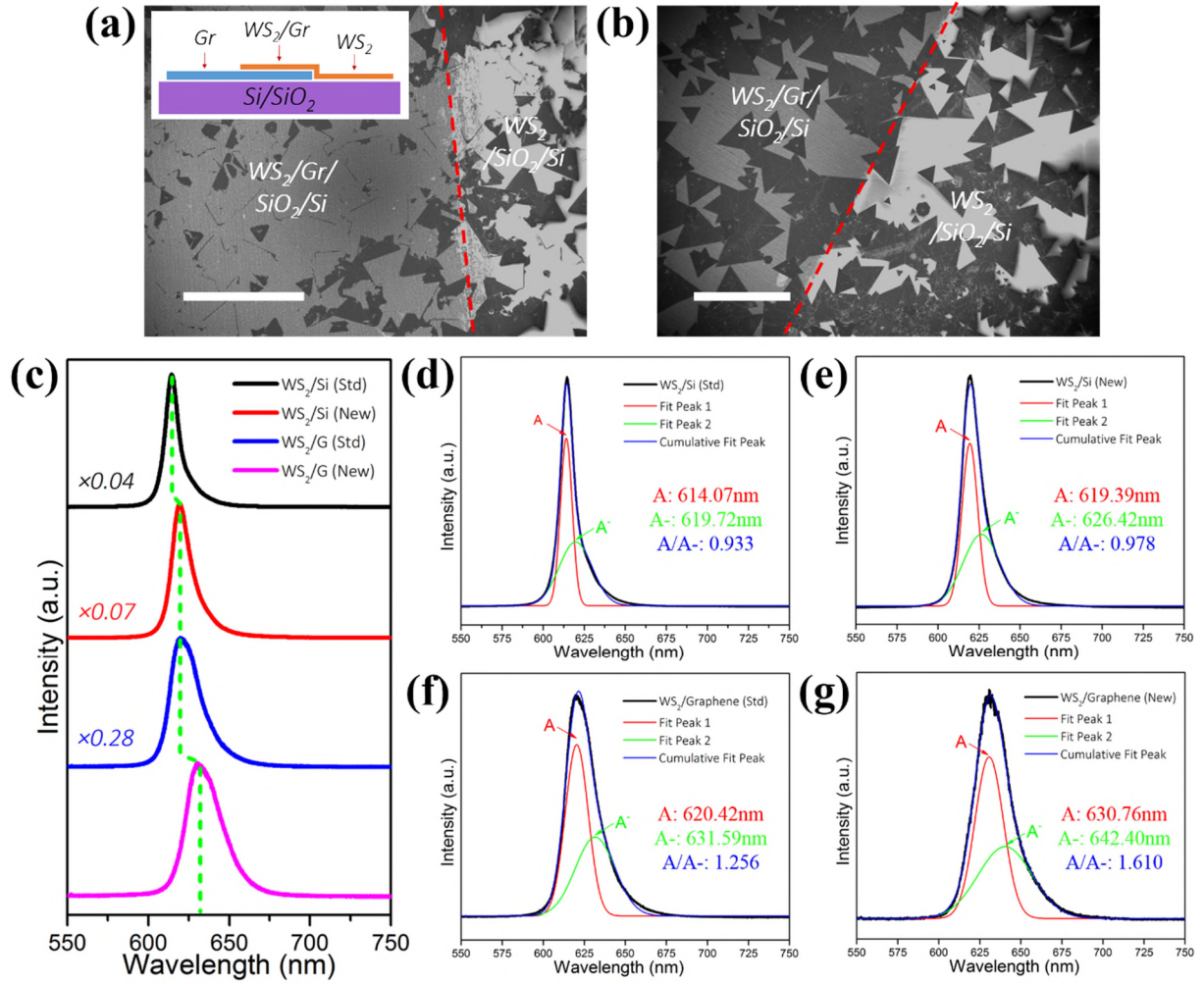


Figure 5. Characterization of WS₂/graphene stacks prepared by either the non-aqueous sliding transfer approach or the standard wet transfer method. SEM images of the WS₂/graphene stack prepared by the non-aqueous sliding transfer approach (a) and the standard wet transfer method (b). Scale bar: 600 μ m. The inset in (a) shows a schematic diagram of the WS₂/graphene stack. (c) PL spectra of the WS₂ on SiO₂/Si and graphene transferred by either the sliding transfer method or the standard wet transfer method, respectively, which highlights the peak shape, intensity and position variation. (d-g) Gaussian fits to the PL peak of transferred WS₂ on SiO₂/Si and graphene using different transfer method, respectively.

The non-aqueous transfer method explored in this work is also suitable for transferring monolayer WS₂ from its growth substrate to other substrates, releasing the strain and also

building multi-layered mixed vertical heterostructures with different stacking order. In Figure 5, we examined the properties of the transferred WS₂ on SiO₂/Si and transferred graphene film. Both the non-aqueous sliding transfer approach and the standard wet transfer method are used for comparison. Graphene only partially covered the substrate and enables comparisons of the WS₂ properties for both the SiO₂ and the graphene region. Figures 5(a) and (b) present the SEM images of transferred WS₂ and WS₂/graphene stack on SiO₂/Si, prepared by the sliding transfer approach and the standard wet transfer method, respectively. The inset in Figure 5(a) shows a schematic of the WS₂/graphene stack. It was found that some of the WS₂ crystals were washed off during the water-based transfer, while all the crystals can be successfully transferred onto other substrates when using the sliding transfer approach. The red dashed line indicates the boundary of the graphene film. We investigated the PL spectra of transferred monolayer WS₂, Figure 5(c), for both transfer methods. The PL intensity of the WS₂ on graphene was quenched for both transfer methods, indicative of strong interactions. However, the non-aqueous transferred sample show larger quenching of the PL signal compared to the aqueous based method, Figure 5(c), indicating stronger interlayer interactions. The peak position of the WS₂ on graphene transferred by the non-aqueous method is also significantly redshifted compared with the aqueous method. The larger quenching and redshift for the WS₂ transferred by the sliding transfer method indicates a cleaner atomic interface between the two layers and results in increased coupling between WS₂ and graphene. As can be seen from Figures 5(d-g), the PL peaks for the WS₂ under different conditions were fitted with two separate Gaussian peaks, which correspond to the neutral exciton (A) and negative trion (A⁻) emission. The energy difference between A and A⁻ is about 20meV for the WS₂ on graphene and 35meV for that on SiO₂/Si, which is consistent with previous reports of binding energy range 20 to 40meV.⁴⁶⁻⁴⁸ In addition, the fitting results show a difference in integrated PL intensity ratio of exciton to

trion (A/A^-), indicating different doping level of WS_2 . It was found that the WS_2 on graphene fabricated by the sliding transfer method has the highest A/A^- , while the WS_2 transferred on SiO_2/Si by the standard aqueous transfer technique has the lowest. It is worth noting that, for both transfer methods, the WS_2 on graphene has a relative higher A/A^- than that on SiO_2/Si , which confirms the higher degree of charged impurities for SiO_2 compared with graphene. Furthermore, for the WS_2 on the same substrate, the A/A^- for the sample transferred by the non-aqueous transfer method is lower than that prepared by aqueous-based one, indicating less contamination is introduced by using the IPA sliding transfer method.

Conclusion

In summary, an alcohol-based transfer technique was developed for transferring 2D materials onto as-grown CVD WS_2 to preserve the inbuilt strain produced during the CVD growth. All the h-BN/ WS_2 , graphene/h-BN/ WS_2 and WS_2 /graphene stacks prepared were characterized by optical microscopy, SEM, Raman spectroscopy and PL measurements, indicating that, by using this method, the as-grown WS_2 domains remain intact on the surface. Stronger interactions between WS_2 on graphene was found when swapping water for IPA, likely resulting from reduced contamination between the layers associated with aqueous impurities. This new method is thought to be particularly useful for fabricating devices that involves transferring one 2D material onto as-grown strained TMDs on sapphire or SiO_2/Si substrates.

Methods

Synthesis of CVD Monolayer WS_2

CVD monolayer WS₂ was prepared using our previously reported CVD approach^{42,43} using Sulphur and WO₃ as precursors. Sulphur and WO₃ were placed in a 1 inch quartz tube running through two furnace systems to provide two heating sections. Vaporized Sulphur and WO₃ were carried by flowing argon gas to the reaction zone, where WO₃ undergoes sulphurization. High quality and large size WS₂ domains with single-layer thickness were grown on Si chips with a layer of 300 nm SiO₂ if appropriate parameters including temperature, argon flow rate and Sulphur introduction time were achieved.

Synthesis of CVD Multilayer h-BN

The multilayer h-BN films were grown on copper foil (25 μm, Alfa Aesar) with the precursor ammonia borane (≥97%, Sigma-Aldrich) using atmospheric pressure CVD (APCVD). The growth was carried out at the temperature of 1000°C for 40 min with argon and hydrogen mixed gas, while the ammonia borane powder was heated to ~80°C. After growth, the furnace was slid away from the sample, which allowed the sample to be fast cooled to room temperature.

Synthesis of CVD graphene

A piece of 25μm thick 99.8% copper (Goodfellow) was first sonicated in diluted hydrochloric acid (HCl) solution (1M), acetone and IPA for 2min, 5min and 5 min, respectively. The CVD growth was then performed at atmospheric pressure and the recipe was based on our previous report.^{49,50} The system was first purged with argon (Ar), hydrogen (H₂) and methane (CH₄) for 30 minutes. The temperature of the furnace was then set to 1060°C at a ramping rate of 50°C/min under a flow of Ar and H₂. The copper was annealed at 1060°C with the same flow rate for 1 hour. Graphene growth was carried out at 1060°C under a mixed flow of Ar, H₂ and

CH₄ for 1 hour. After growth, the furnace was slid away from the sample, which allowed the sample to be fast cooled to room temperature.

Transfer of CVD h-BN, graphene and WS₂

The as-grown 2D materials were first spin-coated with a Poly(methyl methacrylate) (PMMA) scaffold at 4500 rpm for 1 minute and then cured at 180°C for 90 seconds. The CVD-grown h-BN and graphene films were separated from Cu by Ammonium persulfate (APS) etching (0.2 mol/L), while the SiO₂/Si substrate was detached from WS₂ by floating the sample on a 1M Potassium hydroxide (KOH) (Sigma-Aldrich) solution in a water bath at 45°C. The floating film was then transferred to DI water in beakers three times with at least 30min per rinse. The following steps for the standard wet transfer method are suspending the target substrate in the DI water and pushing it towards the floating stack, allowing the surface tension to draw it onto the substrate when pulling it out of the water. The subsequent steps for the non-aqueous transfer method involve dipping a piece of clean cover glass into DI water, pushing it towards the floating film, scooping the film onto the cover glass, wetting the cover glass with some IPA, pipetting some IPA onto the target substrate, which is kept horizontal on the desk, followed by resting one side of the cover glass on the edge of the target substrate and lifting the other side up slightly, allowing the film to slide down very slowly. Finally, for both transfer methods, after being left dry in a fume hood overnight, the transferred sample was baked at 150°C for 15 minutes and then placed in acetone for 2-3 hours to remove PMMA.

Characterization of h-BN/WS₂, graphene/h-BN/WS₂ and WS₂/graphene stack

The structural characteristics of the WS₂ samples and h-BN/WS₂ stack on SiO₂/Si were observed using a scanning electron microscope (Hitachi-4300) under an accelerating voltage

of 3.0 kV. PL measurements of WS₂ and Raman spectroscopy of h-BN was carried out using a JY Horiba LabRAM Aramis imaging confocal Raman microscope under an excitation wavelength of 532 nm.

Acknowledgements

J.H.W. thanks the Royal Society for support. Y.S. acknowledges support from the Sir Richard Stapley Educational Trust and thanks T. Samuels for discussions.

Reference

- (1) Mak, K. F.; Lee, C.; Hone, J.; Shan, J.; Heinz, T. F. Atomically Thin MoS₂: A New Direct-Gap Semiconductor. *Phys. Rev. Lett.* **2010**, *105*, 2–5.
- (2) Radisavljevic, B.; Radenovic, a; Brivio, J.; Giacometti, V.; Kis, a. Single-Layer MoS₂ Transistors. *Nat. Nanotechnol.* **2011**, *6*, 147–150.
- (3) Fang, H.; Chuang, S.; Chang, T. C.; Takei, K.; Takahashi, T.; Javey, A. High-Performance Single Layered WSe₂ P-FETs with Chemically Doped Contacts. *Nano Lett.* **2012**, *12*, 3788–3792.
- (4) Lebègue, S.; Eriksson, O. Electronic Structure of Two-Dimensional Crystals from Ab Initio Theory. *Phys. Rev. B - Condens. Matter Mater. Phys.* **2009**, *79*, 4–7.
- (5) Li, T.; Galli, G. Electronic Properties of MoS₂ Nanoparticles. *J. Phys. Chem. C* **2007**, *111*, 16192–16196.
- (6) Cheiwchanchamnangij, T.; Lambrecht, W. R. L. Quasiparticle Band Structure Calculation of Monolayer, Bilayer, and Bulk MoS₂. *Phys. Rev. B - Condens. Matter Mater. Phys.* **2012**, *85*, 1–4.
- (7) Wang, H.; Yu, L.; Lee, Y.; Shi, Y.; Hsu, A.; Chin, M. L.; Li, L.; Dubey, M.; Kong, J.; Palacios, T. Integrated Circuits Based on Bilayer MoS₂transistors. *Nano Lett.* **2012**, *12*, 4674–4680.
- (8) Zeng, H.; Dai, J.; Yao, W.; Xiao, D.; Cui, X. Valley Polarization in MoS₂ Monolayers by Optical Pumping. *Nat. Nanotechnol.* **2012**, *7*, 490–493.
- (9) Jones, A. M.; Yu, H.; Ghimire, N. J.; Wu, S.; Aivazian, G.; Ross, J. S.; Zhao, B.; Yan, J.; Mandrus, D. G.; Xiao, D.; *et al.* Optical Generation of Excitonic Valley Coherence in Monolayer WSe₂. *Nat. Nanotechnol.* **2013**, *8*, 634–638.
- (10) Sundaram, R. S.; Engel, M.; Lombardo, A.; Krupke, R.; Ferrari, A. C.; Avouris, P.; Steiner, M. Electroluminescence in Single Layer MoS₂. *Nano Lett.* **2013**, *13*, 1416–1421.
- (11) Geim, a K.; Grigorieva, I. V. Van Der Waals Heterostructures. *Nature* **2013**, *499*, 419–425.
- (12) Bernardi, M.; Palummo, M.; Grossman, J. C. Extraordinary Sunlight Absorption and One Nanometer Thick Photovoltaics Using Two-Dimensional Monolayer Materials. *Nano Lett.* **2013**, *13*, 3664–3670.

- (13) Yu, W. J.; Li, Z.; Zhou, H.; Chen, Y.; Wang, Y.; Huang, Y.; Duan, X. Vertically Stacked Multi-Heterostructures of Layered Materials for Logic Transistors and Complementary Inverters. *Nat. Mater.* **2013**, *12*, 246–252.
- (14) Yu, W. J.; Liu, Y.; Zhou, H.; Yin, A.; Li, Z.; Huang, Y.; Duan, X. Highly Efficient Gate-Tunable Photocurrent Generation in Vertical Heterostructures of Layered Materials. *Nat. Nanotechnol.* **2013**, *8*, 952–958.
- (15) Cheng, R.; Li, D.; Zhou, H.; Wang, C.; Yin, A.; Jiang, S.; Liu, Y.; Chen, Y.; Huang, Y.; Duan, X. Electroluminescence and Photocurrent Generation from Atomically Sharp WSe₂/MoS₂ Heterojunction P-N Diodes. *Nano Lett.* **2014**, *14*, 5590–5597.
- (16) Georgiou, T.; Jalil, R.; Belle, B. D.; Britnell, L.; Gorbachev, R. V.; Morozov, S. V.; Kim, Y.-J.; Gholinia, A.; Haigh, S. J.; Makarovskiy, O.; *et al.* Vertical Field-Effect Transistor Based on Graphene-WS₂ Heterostructures for Flexible and Transparent Electronics. *Nat. Nanotechnol.* **2013**, *8*, 100–103.
- (17) Britnell, L.; Ribeiro, R. M.; Eckmann, a; Jalil, R.; Belle, B. D.; Mishchenko, a; Kim, Y.-J.; Gorbachev, R. V.; Georgiou, T.; Morozov, S. V.; *et al.* Strong Light-Matter Interactions in Heterostructures of Atomically Thin Films. *Science* **2013**, *340*, 1311–1314.
- (18) Fang, H.; Battaglia, C.; Carraro, C.; Nemsak, S.; Ozdol, B.; Kang, J. S.; Bechtel, H. a; Desai, S. B.; Kronast, F.; Unal, A. a; *et al.* Strong Interlayer Coupling in van Der Waals Heterostructures Built from Single-Layer Chalcogenides. *Proc. Natl. Acad. Sci. U. S. A.* **2014**, *111*, 6198–6202.
- (19) Huo, N.; Kang, J.; Wei, Z.; Li, S.-S.; Li, J.; Wei, S.-H. Novel and Enhanced Optoelectronic Performances of Multilayer MoS₂-WS₂ Heterostructure Transistors. *Adv. Funct. Mater.* **2014**, *24*, 7025–7031.
- (20) Liu, K.; Yan, Q.; Chen, M.; Fan, W.; Sun, Y.; Suh, J.; Fu, D.; Lee, S.; Zhou, J.; Tongay, S.; *et al.* Elastic Properties of Chemical-Vapor-Deposited Monolayer MoS₂, WS₂, and Their Bilayer Heterostructures. *Nano Lett.* **2014**, *14*, 5097–5103.
- (21) Tongay, S.; Fan, W.; Kang, J.; Park, J.; Koldemir, U.; Suh, J.; Narang, D. S.; Liu, K.; Ji, J.; Li, J.; *et al.* Tuning Interlayer Coupling in Large-Area Heterostructures with CVD-Grown MoS₂ and WS₂ Monolayers. *Nano Lett.* **2014**, *14*, 3185–3190.
- (22) Hong, X.; Kim, J.; Shi, S.-F.; Zhang, Y.; Jin, C.; Sun, Y.; Tongay, S.; Wu, J.; Zhang, Y.; Wang, F. Ultrafast Charge Transfer in Atomically Thin MoS₂/WS₂ Heterostructures. *Nat. Nanotechnol.* **2014**, *9*, 682–686.
- (23) Loan, P. T. K.; Zhang, W.; Lin, C.-T.; Wei, K.-H.; Li, L.-J.; Chen, C.-H. Graphene/MoS(2) Heterostructures for Ultrasensitive Detection of DNA Hybridisation. *Adv. Mater.* **2014**, *26*, 4838–4844.

- (24) Wang, S.; Wang, X.; Warner, J. H.; Al, W. E. T. All Chemical Vapour Deposition Growth of MoS₂ : H-BN Vertical van Der Waals Heterostructures. *ACS Nano* **2015**, *9*, 5246–5254.
- (25) Shi, Y.; Zhou, W.; Lu, A.; Fang, W.; Lee, Y.; Hsu, A. L.; Kim, S. M.; Kim, K. K.; Yang, H. Y.; Li, L.-J.; *et al.* Van Der Waals Epitaxy of MoS₂ Layers Using Graphene as Growth Templates. *Nano Lett.* **2012**, *12*, 2784–2791.
- (26) Gong, Y.; Lin, J.; Wang, X.; Shi, G.; Lei, S.; Lin, Z.; Zou, X.; Ye, G.; Vajtai, R.; Yakobson, B. I.; *et al.* Vertical and in-Plane Heterostructures from WS₂/MoS₂ Monolayers. *Nat. Mater.* **2014**, *13*, 1135–1142.
- (27) Heo, H.; Sung, J. H.; Jin, G.; Ahn, J.-H.; Kim, K.; Lee, M.-J.; Cha, S.; Choi, H.; Jo, M.-H. Rotation-Misfit-Free Heteroepitaxial Stacking and Stitching Growth of Hexagonal Transition-Metal Dichalcogenide Monolayers by Nucleation Kinetics Controls. *Adv. Mater.* **2015**, *27*, 3803–3810.
- (28) Schneider, G. F.; Calado, V. E.; Zandbergen, H.; Vandersypen, L. M. K.; Dekker, C. Wedging Transfer of Nanostructures. *Nano Lett.* **2010**, *10*, 1912–1916.
- (29) Gurarslan, A.; Yu, Y.; Su, L.; Yu, Y.; Suarez, F.; Yao, S.; Zhu, Y. Surface-Energy-Assisted Perfect Transfer of Centimeter-Scale Films onto Arbitrary Substrates. *ACS Nano* **2014**, 11522–11528.
- (30) Xu, Z.; Zhang, Y.; Lin, S.; Zheng, C.; Zhong, Y. L.; Xia, X.; Li, Z.; Sophia, P. J.; Fuhrer, M. S.; Cheng, Y.-B.; *et al.* Synthesis and Transfer of Large-Area Monolayer WS₂ Crystals: Moving Toward the Recyclable Use of Sapphire Substrates. *ACS Nano* **2015**, *9*, 6178–6187.
- (31) Lee, Y. H.; Yu, L.; Wang, H.; Fang, W.; Ling, X.; Shi, Y.; Lin, C. Te; Huang, J. K.; Chang, M. T.; Chang, C. S.; *et al.* Synthesis and Transfer of Single-Layer Transition Metal Disulfides on Diverse Surfaces. *Nano Lett.* **2013**, *13*, 1852–1857.
- (32) Li, X.; Zhu, Y.; Cai, W.; Borysiak, M.; Han, B.; Chen, D.; Piner, R. D.; Colombo, L.; Ruoff, R. S. Transfer of Large-Area Graphene Films for High-Performance Transparent Conductive Electrodes. *Nano Lett.* **2009**, *9*, 4359–4363.
- (33) Suk, J. W.; Kitt, A.; Magnuson, C. W.; Hao, Y.; Ahmed, S.; An, J.; Swan, A. K.; Goldberg, B. B.; Ruoff, R. S. Transfer of CVD-Grown Monolayer Graphene onto Arbitrary Substrates. *ACS Nano* **2011**, *5*, 6916–6924.
- (34) Wang, Y.; Zheng, Y.; Xu, X.; Dubuisson, E.; Bao, Q.; Lu, J.; Loh, K. P. Electrochemical Delamination of CVD-Grown Graphene Film: Toward the Recyclable Use of Copper Catalyst. *ACS Nano* **2011**, *5*, 9927–9933.

- (35) Castellanos-Gomez, A.; Roldán, R.; Cappelluti, E.; Buscema, M.; Guinea, F.; Van Der Zant, H. S. J.; Steele, G. a. Local Strain Engineering in Atomically Thin MoS₂. *Nano Lett.* **2013**, *13*, 5361–5366.
- (36) Hui, Y. Y.; Liu, X.; Jie, W.; Chan, N. Y.; Hao, J.; Hsu, Y. Te; Li, L. J.; Guo, W.; Lau, S. P. Exceptional Tunability of Band Energy in a Compressively Strained Trilayer MoS₂ Sheet. *ACS Nano* **2013**, *7*, 7126–7131.
- (37) Liu, Z.; Amani, M.; Najmaei, S.; Xu, Q.; Zou, X.; Zhou, W.; Yu, T.; Qiu, C.; Birdwell, a. G.; Crowne, F. J.; *et al.* Strain and Structure Heterogeneity in MoS₂ Atomic Layers Grown by Chemical Vapour Deposition. *Nat. Commun.* **2014**, *5*, 5246.
- (38) Conley, H. J.; Wang, B.; Ziegler, J. I.; Haglund, R. F.; Pantelides, S. T.; Bolotin, K. I. Bandgap Engineering of Strained Monolayer and Bilayer MoS₂. *Nano Lett.* **2013**, *13*, 3626–3630.
- (39) Wang, Y.; Cong, C.; Qiu, C.; Yu, T. Raman Spectroscopy Study of Lattice Vibration and Crystallographic Orientation of Monolayer mos₂ under Uniaxial Strain. *Small* **2013**, *9*, 2857–2861.
- (40) He, K.; Poole, C.; Mak, K. F.; Shan, J. Experimental Demonstration of Continuous Electronic Structure Tuning via Strain in Atomically Thin MoS₂. *Nano Lett.* **2013**, *13*, 2931–2936.
- (41) Feng, J.; Qian, X.; Huang, C.; Li, J. Strain-Engineered Artificial Atom as a Broad-Spectrum Solar Energy Funnel. *Nat. Photonics* **2012**, *6*, 866–872.
- (42) Rong, Y.; Fan, Y.; Leen Koh, A.; Robertson, A. W.; He, K.; Wang, S.; Tan, H.; Sinclair, R.; Warner, J. H. Controlling Sulphur Precursor Addition for Large Single Crystal Domains of WS₂. *Nanoscale* **2014**, *6*, 12096–12103.
- (43) Rong, Y.; He, K.; Pacios, M.; Robertson, A. W.; Bhaskaran, H.; Warner, J. H. Controlled Preferential Oxidation of Grain Boundaries in Monolayer Tungsten Disulfide for Direct Optical Imaging. *ACS Nano* **2015**, *9*, 3695–3703.
- (44) He, Z.; Sheng, Y.; Rong, Y.; Lee, G.; Li, J.; Warner, J. H. Layer-Dependent Modulation of Tungsten Disulfide Photoluminescence by Lateral Electric Fields. *ACS Nano* **2015**, *9*, 2740–2748.
- (45) Bhanu, U.; Islam, M. R.; Tetard, L.; Khondaker, S. I. Photoluminescence Quenching in Gold - MoS₂ Hybrid Nanoflakes. *Sci. Rep.* **2014**, *4*, 5575.
- (46) Zhu, B.; Chen, X.; Cui, X. Exciton Binding Energy of Monolayer WS₂. *Sci. Rep.* **2014**, *5*, 9218.

- (47) Mitiglu, a. a.; Plochocka, P.; Jadcak, J. N.; Escoffier, W.; Rikken, G. L. J. a; Kulyuk, L.; Maude, D. K. Optical Manipulation of the Exciton Charge State in Single-Layer Tungsten Disulfide. *Phys. Rev. B - Condens. Matter Mater. Phys.* **2013**, *88*, 1–5.
- (48) Chernikov, A.; Berkelbach, T. C.; Hill, H. M.; Rigosi, A.; Li, Y.; Aslan, O. B.; Reichman, D. R.; Hybertsen, M. S.; Heinz, T. F. Exciton Binding Energy and Nonhydrogenic Rydberg Series in Monolayer WS₂. *Phys. Rev. Lett.* **2014**, *113*, 076802.
- (49) Wu, Y. A.; Fan, Y.; Speller, S.; Creeth, G. L.; Sadowski, J. T.; He, K.; Robertson, A. W.; Allen, C. S.; Warner, J. H. Large Single Crystals of Graphene on Melted Copper Using Chemical Vapor Deposition. *ACS Nano* **2012**, *6*, 5010–5017.
- (50) Sheng, Y.; Rong, Y.; He, Z.; Fan, Y.; Warner, J. H. Uniformity of Large-Area Bilayer Graphene Grown by Chemical Vapor Deposition. *Nanotechnology* **2015**, *26*, 395601.

TOC

